DYNAMIC OUTGASSING

Oswald Gröbner
CERN, Geneva, Switzerland

Abstract
Outgassing stimulated by photons, ions and electrons created by high-energy and high-intensity particle beams in accelerators and storage rings represents a serious limitation for the design of vacuum systems. Synchrotron-radiation-induced desorption is particularly important for intense light sources and high current storage rings. Gas desorption-induced by beam generated ions was a serious limitation to the performance of the Intersecting Proton Storage Rings (ISR) at CERN in the past and is a major concern for the vacuum system design of the Large Hadron Collider.

1. SYNCHROTRON RADIATION-INDUCED DESORPTION

In high-energy, high-intensity accelerators and storage rings for electrons and positrons, the particle beams emit intense synchrotron radiation in a forward-directed narrow cone. This energetic photon flux produces strong outgassing from the vacuum system and thus a large dynamic pressure increase, which limits the beam lifetime in the machine and may cause increased background in the colliding-beam experiments. For the first time a significant level of synchrotron radiation will also occur with the 7-TeV proton beams in the LHC.

1.1 Basic equations for synchrotron radiation

The equations required to evaluate the vacuum conditions with synchrotron radiation for electrons or positrons [1] are:

Total radiated power (W):

$$P_\gamma = 88.6 \frac{E^4 I}{\rho} \tag{1}$$

where E (GeV) is the beam energy, I (mA) the beam current and ρ (m) the bending radius. The critical energy of the S.R. spectrum (eV) is given by

$$\varepsilon_c = 2.2 \cdot 10^3 \frac{E^3}{\rho} \ . \tag{2}$$

The total photon flux (s^{-1}) around the machine circumference is

$$\dot{\Gamma} = 8.08 \cdot 10^{17} IE \tag{3}$$

and the linear photon flux ($m^{-1}\ s^{-1}$)

$$\frac{d\dot{\Gamma}}{ds} = 1.28 \cdot 10^{17} \frac{IE}{\rho} \ . \tag{4}$$

The gas flow due to photon induced desorption

$$Q = \eta \dot{\Gamma} \tag{5}$$

where η is the molecular desorption yield (molecules per photon) averaged over all photon energies. The total gas load including the contribution from thermal outgassing Q_o (Torr l s^{-1}) is

$$Q = \mathrm{K}\eta I E + Q_o \tag{6}$$

where the constant K converts from molecules to pressure units (e.g. K = 2.8 10^{-20} Torr l/molecule at 273K). The total dynamic pressure is

$$P_{dyn} = \frac{Q}{S} \ . \tag{7}$$

The instantaneous dynamic pressure increases proportionally with the beam intensity and this quantity is generally referred to as the dynamic pressure rise (Torr/mA):

$$\frac{\Delta P}{I} = \frac{Q - Q_o}{S} \tag{8}$$

which depends on the pumping speed of the vacuum system. Since the gas desorption occurs all around the bending sections of the machine, a distributed pumping system using 'linear integrated' pumps has significant advantages over individual, lumped pumps.

During machine operation, ‘beam cleaning’ or ‘beam scrubbing’ of the vacuum system effectively reduces the molecular desorption yield by several orders of magnitude. Since it would be very expensive to build a vacuum system with sufficient pumping speed to guarantee the required beam lifetime at the start-up, most synchrotron light sources and storage rings take advantage of the beam cleaning process. It is an accepted design concept that the required vacuum performance will be achieved after an initial conditioning time only.

The cleaning time or, more specifically, the integrated beam dose which is required to reduce the molecular desorption yield from its initial large value, can be estimated with good accuracy using the exponential dependence on the beam dose D (mA h)

$$\eta = \eta_o \, D^{-a} . \tag{9}$$

The exponent a is found to vary between 0.6 to ~1 depending on the specific machine [2–4]. The observed clean-up for LEP is shown in Fig. 1. The detailed evolution of the dynamic pressure rise in LEP depends on the combined effect of the clean-up of the vacuum system and of the saturation of the linear getter pumps (NEG). The indicated straight line with a slope of –1 corresponds to the measurements with a newly activated getter and hence a constant, maximum pumping speed.

Photon stimulated molecular desorption has been attributed to a two step process [5, 6]:

in the first step photons produce photo-electrons and secondary electrons

subsequently secondary-electrons excite strongly-bound molecules, which may desorb spontaneously. This model is strongly supported by measurements that have shown a very close correlation between gas desorption and photoelectrons produced [7].

1.2 Molecular-desorption yields for various vacuum chamber materials

For the design of vacuum systems the most important parameter is the desorption yield for the relevant conditions of synchrotron-radiation spectrum, angle of incidence and vacuum chamber materials. Stimulated by the need to obtain reliable input data for the design of vacuum systems,

extensive investigations have been made using the experimental system shown in Fig. 2. This set-up allows the measurement of the instantaneous desorption yield as well as its evolution with beam dose,

the dependence on the synchrotron radiation spectrum (critical energy) and the angle of incidence. A detailed description of this system which was first installed on an external photon beam line at the DCI storage ring in ORSAY, France can be found in Ref. [1].

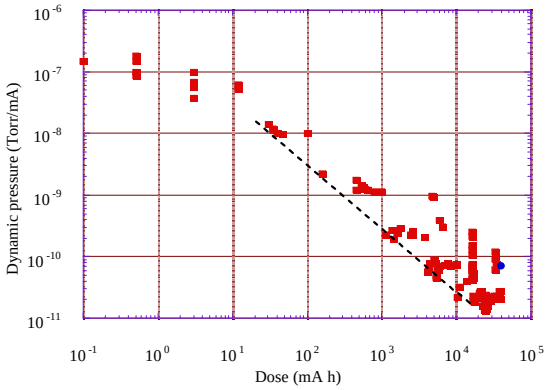

Fig. 1 Beam cleaning during the first running period of LEP.

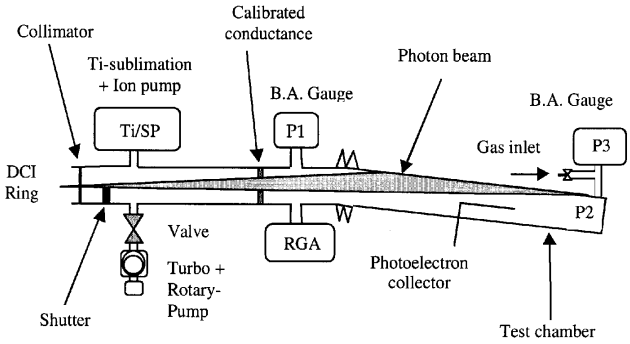

Fig. 2 Experimental system to measure synchrotron radiation-induced desorption.

The photon beam is extracted from a bending magnet and passes through a set of vertical and horizontal collimators which precisely define the total photon flux which enters the experiment. Due to the vertical divergence of synchrotron radiation the vertical collimation has been chosen sufficiently large so as not to attenuate the photon spectrum at low photon energies (e.g. below about 5 eV in the DCI set-up). To study the effect of angle of incidence, a set of bellows has been introduced so that the test chamber can be pivoted in the horizontal plane. Total and partial pressure measurements are done with a combination of calibrated total pressure gauges and a calibrated quadrupole mass spectrometer. To correlate photoelectrons with molecular desorption, an electrically biased wire electrode has been installed in some of the test chambers.

With the growing importance of reliable input data for the design of future synchrotron light sources and e^+e^- storage rings, similar experiments have been installed in several other synchrotron light sources at KEK Japan, BNL USA, EPA at CERN, INP Russia and ESRF France. The results obtained with this set-up can be considered as representative for a real machine vacuum system. However, it should be noted that the measurement gives a net desorption yield since only the net amount of gas leaving a test chamber through the calibrated conductance can be observed. Furthermore, with grazing photon incidence, a fraction of the photons is reflected from the region of the primary impact and may not desorb molecules. These reflected photons may nevertheless contribute to the gas desorption when they strike the end face of the test chamber under near perpendicular incidence. For a more accurate measurement, the amount of reflected photons should be estimated and the molecular yields corrected for this effect.

1.3 Measured desorption yields

Measurements at DCI have been made with a critical photon energy between 0.8 and 3.75 keV and 11 mrad grazing photon incidence on a 3.5-m long test chamber. A selection of results is shown in Figs. 3 to 6 respectively referring to *in-situ* baked (between 150°C and 300°C) vacuum chambers made of aluminium alloy, untreated stainless steel and stainless steel baked under vacuum at 950°C (vacuum degassed) as a pre-treatment and finally OFHC-copper. Additional results for an unbaked stainless steel chamber may be found Ref. [3]. In order to facilitate the scaling of these data to the specific conditions in other accelerators, the beam dose has been expressed in accumulated photons per m of test chamber rather than in machine mA hours.

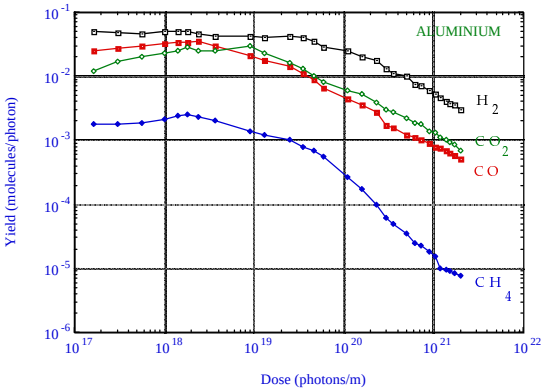

Fig. 3 Molecular desorption yields for aluminium alloy.

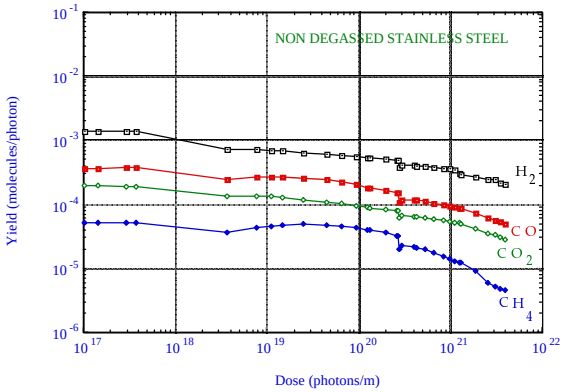

Fig. 4 Molecular desorption yields for stainless steel.

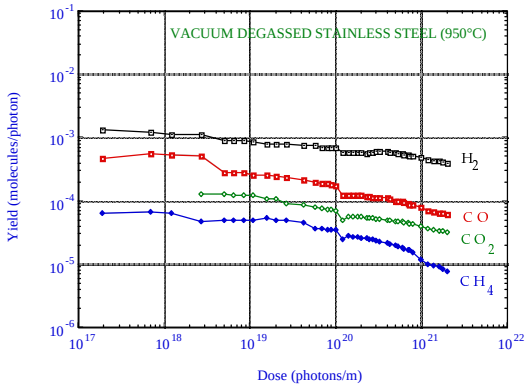

Fig. 5 Molecular desorption yields for vacuum fired stainless steel.

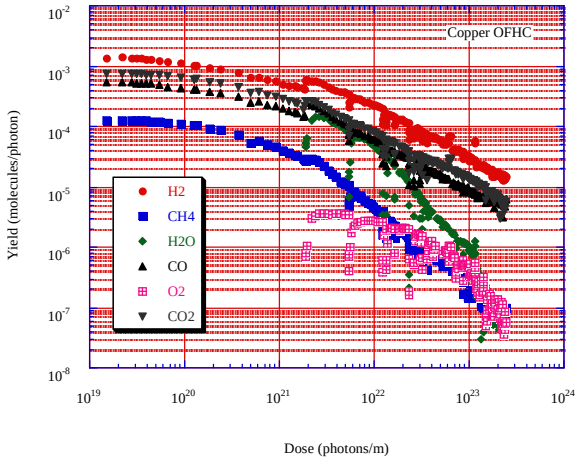

Fig. 6 Molecular desorption yields for OFHC copper.

The total duration of the photon exposures in these measurements ranges from some 24 hours to many weeks in the case of Fig. 6. Therefore, each individual plot represents many successive exposures with intermittent periods when the pressure in the test chamber has time to recover. In spite of these interruptions, the dynamic pressure evolution and the molecular desorption yields derived from it follow a steadily decreasing trend.

1.4 Energy dependence of the molecular-desorption yield

The dependence of the desorption yield on the critical energy of the S.R. has been measured over a range of energies and for different vacuum chambers. Basically one can expect a lower threshold at which the photon energy is insufficient to produce photoelectrons (~5 eV). With increasing energy, photons penetrate progressively deeper into the surface such that the escape probability for electrons is reduced. This effect should lead to a decreasing desorption efficiency per total number of photons. For very high photon energies, above several hundred keV and even MeV as in LEP, the Compton cross section dominates over the photo effect. Compton scattering will produce a shower of energetic recoil electrons and an increasing number of scattered secondary photons. The global effect, as seen in LEP at beam energies above 50 GeV is an increasing desorption yield. Figure 7 shows a compilation of desorption data collected from various experiments and machines and covering the range of critical photon energies from 12 eV up to several hundred keV. The data referring to a

particular machine have been obtained under the same conditions and should reflect the energy variation for this particular system while the data from different experiments may not be directly comparable and have therefore been plotted in arbitrary units. At very low energies, representative of the situation in the LHC [8], the yield increases strongly with energy.

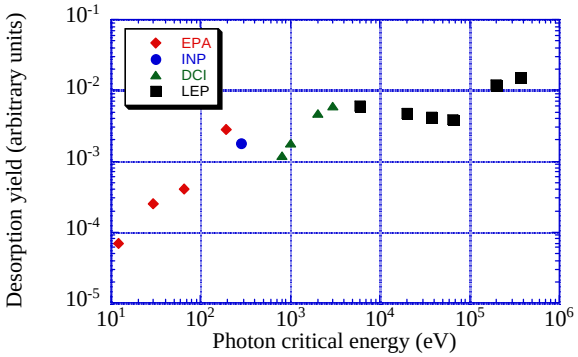

Fig. 7 Relative desorption efficiency as a function of the critical photon energy.

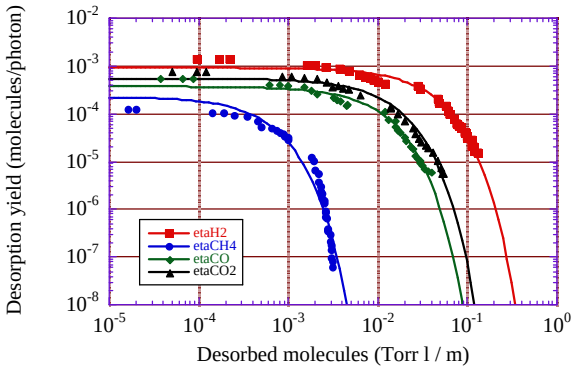

Fig. 8 Integral gas load for an OFHC copper chamber.

1.5 Integral desorbed-gas load

A quantity, which is particularly relevant for a getter-pumped vacuum system in order to estimate the intervals when the getter will have to be reconditioned, is the integral amount of desorbed gas during the cleaning process. This quantity can be obtained by integrating the respective cleaning curves. For the OFHC copper chamber the result of the integration is shown in Fig. 8. The observed decrease of the desorption yield η as function of the gas load Q (Torr l/m) can be described closely by the exponential expression:

$$\eta = \eta_0 \, e^{-\frac{Q}{Q_0}} \quad . \tag{10}$$

The respective values of the two parameters η_0 and Q_0 for different gas species are given in Table 1. The first line gives the monolayer capacity, which has been used to calculate the value of Q_0 in the last line.

Table 1
Parameters for OFHC copper

	H_2	**CH_4**	**CO**	**CO_2**
Molecules (cm^{-2}/monolayer)	$1.8\ 10^{15}$	$1.2\ 10^{15}$	$1.0\ 10^{15}$	$9.6\ 10^{14}$
η_0 (molecules/photon)	$9.2\ 10^{-4}$	$2.3\ 10^{-4}$	$3.7\ 10^{-4}$	$5.5\ 10^{-4}$
Q (Torr l/m)	$3.0\ 10^{-2}$	$4.5\ 10^{-4}$	$8.4\ 10^{-3}$	$1.1\ 10^{-2}$
Q_0 (monolayers)	0.13	$2.9\ 10^{-3}$	$6.5\ 10^{-2}$	$8.9\ 10^{-2}$

It can be seen that, e.g. for a baked copper chamber, the total amount of gas which needs to be pumped remains well within the capacity of commercial getter pumps. By comparison, the gas load for an aluminium alloy vacuum chamber is more than one order of magnitude larger but in spite of this larger load it has not caused any vacuum limitations during LEP operation [9].

1.6 Observations of time-dependent effects

Detailed measurements have shown that molecules desorb not only from the directly illuminated region but from the entire inner surface due to the scattered/reflected photons as well as secondary electrons. As a consequence, a vacuum chamber must be cleaned over its full perimeter and not only along a narrow directly illuminated strip.

A pronounced and persistent wall pumping effect has been observed after prolonged photon exposure, which translates into a molecular sticking probability of about 10^{-4}. Due to this pumping effect, molecules may re-adsorb several times on the walls before leaving the system. Therefore, the system in Fig. 2 measures an effective, net yield rather than a true, intrinsic desorption rate.

Meta-stable, excited molecules accumulate and recombine on the surface producing new species, e.g. H_2O and O_2 which have been observed after a prolonged photon exposure. This effect is illustrated in Fig. 9 where it is shown that several hours of exposure may be required until the desorption process reaches a steady state.

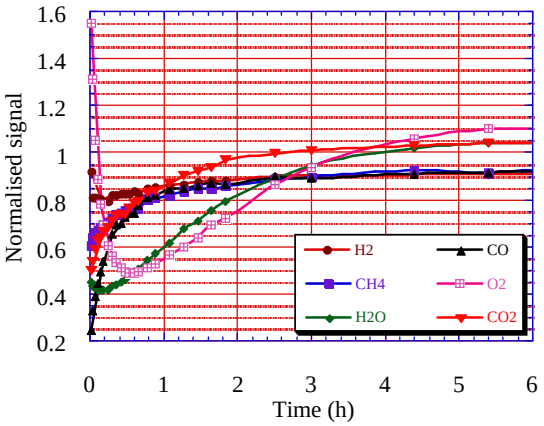

Fig. 9 Time-dependent partial pressures at the beginning of an irradiation period following an interruption of several hours.

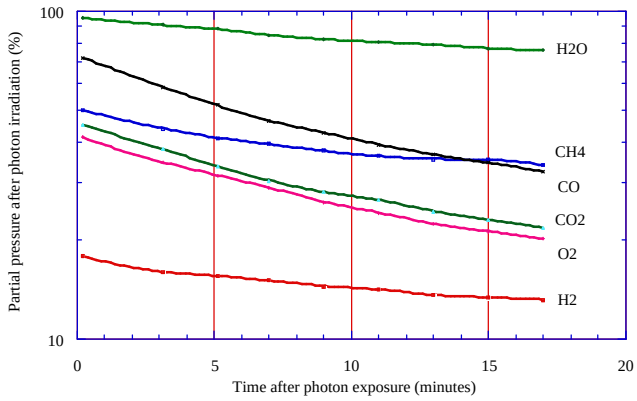

Fig. 10 Time-dependent partial pressures following an irradiation period.

The inverse process when the photon beam is stopped after a long irradiation period is shown in Fig. 10. While certain molecular species show a large instantaneous reduction, several other gases such as H_2O, decrease by a very small amount only and continue to evolve over a very long period of time. Indeed it may take many hours and even days until the system comes back to its pre-irradiation conditions. Based on these observations, synchrotron radiation stimulated desorption can be separated into a

- prompt component, characterised by the fact that desorption stops immediately with the photon irradiation and a

- delayed component, equivalent to an increased level of thermal desorption persisting long after the photon irradiation and characterised by the appearance of 'new' molecular species. The best illustration for this delayed component may be O_2 in Fig. 9. This species accumulates during the irradiation free period preceding the measurement since its initial desorption yield is by a factor of 1.6 higher than its steady state value.

Photon stimulated desorption of H_2 can be described very closely by a diffusion model from the bulk to the surface [10].

2. ION-INDUCED DESORPTION

In storage rings with intense, positively-charged beams of protons and positrons the pressure can increase due to ion-induced desorption from the walls of the beam pipe. Ions created from the residual gas are repelled by the positive space-charge potential and are accelerated towards the wall.

Ions may gain energies of several hundred eV per ampere of circulating current and are thus very effective for desorbing strongly-bound gas molecules. Since the rate of ionisation is proportional to the gas density an avalanche process may occur resulting in a continuously increasing pressure, see Fig. 11.

The total flux of desorbed gas into the vacuum system is:

$$Q = \eta\,\sigma\;P\frac{I}{e} + Q_o \tag{11}$$

where η is the molecular desorption yield (molecules/ion), σ the ionisation cross section of the residual gas molecules, P the pressure, I the average beam current, e the unit charge and Q_o is the thermal outgassing rate from the wall.

The balance of gas desorbed by the beam and removed by external pumps, S is given by

$$PS = \eta\sigma\frac{I}{e}P + Q_O \tag{12}$$

and therefore

$$P = \frac{Q_o}{S - \eta\sigma\dfrac{I}{e}}\ . \tag{13}$$

One finds that the pressure increases with beam current and that above a critical value no equilibrium pressure exists:

$$(\eta I)_{crit} = \frac{e\;S}{\sigma}\ . \tag{14}$$

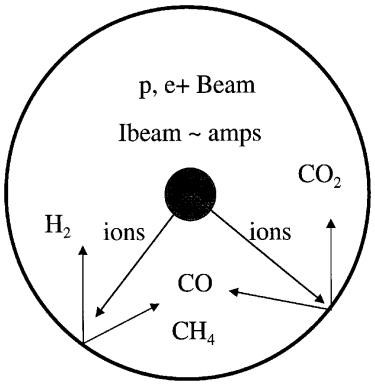

Fig. 11 Beam induced desorption mechanism.

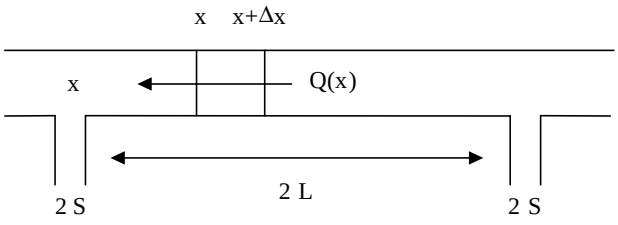

Fig. 12 Linear vacuum system with ion-induced desorption.

2.1 Parameters which determine vacuum stability

Ionisation cross sections for some common gas species are listed in Table 2. The values have been calculated for the beam energies in the ISR and for LHC using Ref. [11].

Table 2
Ionisation cross sections

	Ionisation cross-section (in 10^{-18} cm^2)	
Gas	**26 GeV**	**7000 GeV**
H_2	0.22	0.37
He	0.23	0.38
CH_4	1.2	2.1
CO	1.0	1.8
Ar	1.1	2.0
CO_2	1.6	2.8

2.2 Effective pumping speed S_{eff}

The pumping speed which is required to compensate the desorption by ions depends strongly on the configuration of the vacuum system: For a periodically pumped, linear vacuum system with the layout as in Fig. 12, the vacuum stability can be calculated as shown below [12]. The addition of distributed pumping, e.g. by a continuous, linear getter pump or by cryopumping in a cold-bore vacuum system can be implemented as a straightforward extension of the mathematical formalism.

Gas flow $Q(x)$ [Torr m^3 s^{-1}]

Specific linear outgassing rate: $q(x)$ [Torr m^2 s^{-1}]

Specific molecular conductance of the vacuum chamber: c [m^4 s^{-1}]

Pumping speed S [m^3 s^{-1}]

Ion-induced desorption coefficient b [m^2 s^{-1}] where

$$b = \sigma \eta \frac{I}{e} \tag{15}$$

with I the beam current, e the electron charge, σ the ionisation cross section and η the molecular desorption yield which is expressed here in molecules/ion.

In stationary conditions, the pressure is given by

$$c \frac{d^2P}{dx^2} + bP + q = 0 \ . \tag{16}$$

Boundary conditions for a uniform, periodic vacuum system with pumps (each pump has the speed $2S$) at a regular distance $2L$ are given by:

$$c \left[\frac{dP}{dx} \right]_{x=\pm L} = \mp S P[\pm L] \ . \tag{17}$$

Three types of solutions exist for this system, which depend on the range of the parameter b:

For $\boldsymbol{b = 0}$, one obtains the usual parabolic pressure distribution for a periodically pumped system:

$$P(x) = q\left(\frac{2Lx - x^2}{2c} + \frac{L}{S} \right) . \tag{18}$$

For $\boldsymbol{b > 0}$, the solution has the form

$$P[x] = \frac{q}{b}\left[\frac{\cos[\sqrt{b/c}\ x]}{\cos[\sqrt{b/c}\ L] - \frac{\sqrt{bc}}{S}\sin[\sqrt{b/c}\ L]} - 1\right] . \tag{19}$$

A finite solution exists as long as:

$$\cos[\sqrt{b/c}\ L] - \frac{\sqrt{bc}}{S}\sin[\sqrt{b/c}\ L] > 0 \ . \tag{20}$$

The limit of vacuum stability, i.e. the largest stable value for the parameter *b* corresponds to the first root of the transcendental equation

$$L\sqrt{b/c}\ \tan[L\sqrt{b/c}] = \frac{SL}{c} \tag{21}$$

and can be computed numerically. Nevertheless, an upper limit for *b* exists when the vacuum system is strongly conductance limited (*S* and *L* very large or c very small), which can be obtained simply from the argument when the tangent goes to infinity:

$$b_{\max} = \frac{\pi^2}{4}\frac{c}{L^2} \ . \tag{22}$$

The critical beam current for this limiting condition is

$$(\eta I)_{crit} = \frac{\pi^2}{4}\frac{e\ c}{\sigma\ L^2} \ . \tag{23}$$

For any practical case, the critical current will be lower but any ‘well designed’ vacuum system should fall within 30% of this simplified condition.

Finally for $\boldsymbol{b < 0}$, the pressure decreases since the beam acts like an ion-pump — beam pumping. The pressure distribution follows a hyperbolic function and remains always stable. Numerically the ‘pumping speed’ of the beam can be calculated from the expression

$$S_{beam} = \frac{\sigma\kappa}{e} I \ (\mathrm{m^2\,s^{-1}}) \tag{24}$$

where κ represents the probability that an incident ion is captured at the wall. Beam pumping increases with the beam current and has been observed frequently, but not systematically, in the ISR with currents of up to 60 A [13]. The pumping depends directly on the capture probability of the ions on the wall and a rough estimate of this effect may be derived from the pumping speed of a commercial ion pump as $\kappa \sim 0.1$ [14].

2.3 Molecular-desorption yield

Desorption yields which are measured in a laboratory system [15] and in a real machine where the bombarding ions are generated directly from the residual gas, are related to each other by the condition

$$\eta_m = \eta_{lab} - \kappa \ . \tag{25}$$

In the case where $\kappa > \eta_{lab}$, the effective yield is negative and the beam will act as a pump. The upper limit for κ is unity corresponding to the situation when all ions are implanted and pumped on the wall of the vacuum system. In reality, the capture probability will be considerably less than unity and one may expect that it depends on the surface conditions, the type of ions and on the ion energy.

Ion-induced desorption yields have been measured for a number of vacuum chamber materials and for a large variety of vacuum treatments [16]. The most relevant data for designing future accelerator vacuum systems, the desorption yields for unbaked and for *in-situ* baked stainless steel chambers, are shown in Figs. 13 and 14 as a function of the ion energy [17].

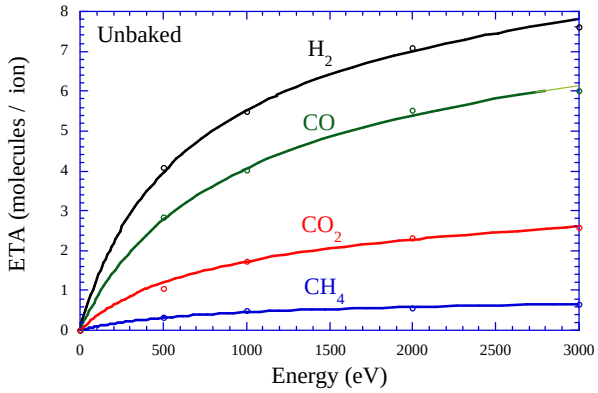

Fig. 13 Desorption yields for unbaked stainless steel as a function of incident ion energy.

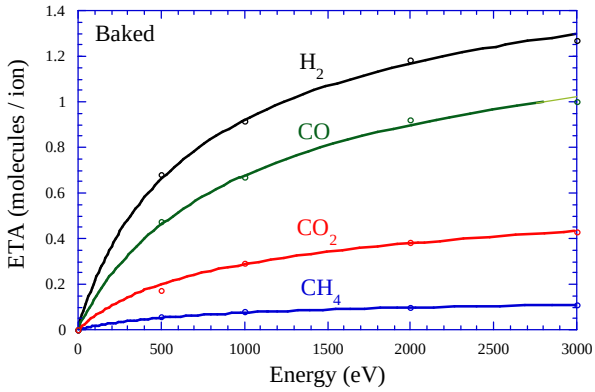

Fig. 14 Desorption yields for baked stainless steel as a function of ion energy.

The most significant permanent improvement among a variety of possible treatments has been achieved by using an argon ion glow discharge followed by an *in-situ* bakeout, see Fig. 15. A glow discharge treatment without subsequent *in-situ* bakeout of the vacuum system results only in a small, often insufficient improvement [18].

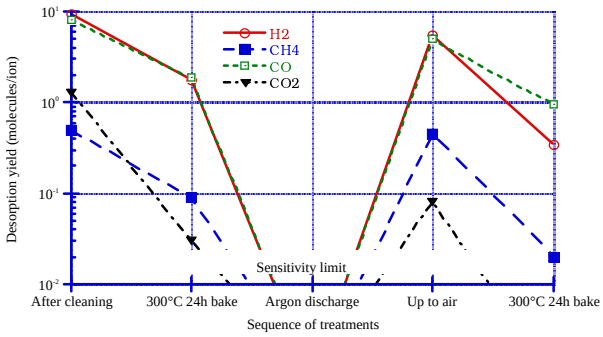

Fig. 15 Effect of various treatments on the ion-induced desorption coefficients.

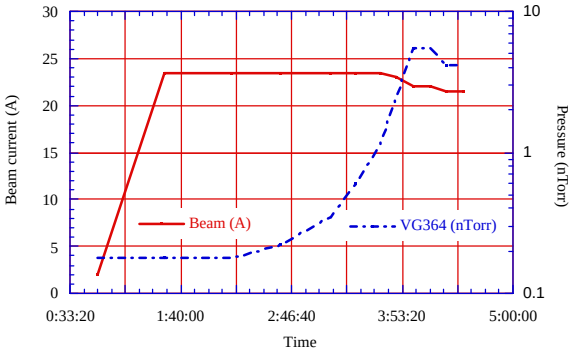

Fig. 16 Pressure instability during beam stacking in the ISR.

2.4 Vacuum stability in a cold bore system with cryosorbing walls (LHC)

In a cryogenic vacuum system with cold walls molecules are cryopumped with high efficiency directly onto the cold bore. The pumping speed per unit length is

$$S_{eff} = \frac{1}{4}\bar{v}\, s\, F \tag{26}$$

with $\bar{v}$ the mean molecular velocity, s the sticking probability of molecules on the wall and F the surface area per unit length.

With a cold beam pipe of radius r_p, the stability limit is

$$(\eta I)_{crit} = \frac{\pi}{2}\bar{v}\, s\, r_p\, \frac{e}{\sigma} \tag{27}$$

and for s~1 the critical current should be very large, of the order of kA [19, 8]. However, this large stability limit can be offset by two factors:

Firstly, the sticking probability can be much smaller than unity

Secondly, the molecular desorption yield for condensed gas, specifically for H_2 accumulating on the cold bore, can become very large. Values of up to 10^4 molecules per ion have been measured in the laboratory [20]. However, as has been demonstrated within the on-going LHC vacuum studies, cryosorbed hydrogen which is irradiated by photons will desorb with a very high efficiency. This strong recycling effect counteracts the accumulation of hydrogen on the wall of the LHC beam screen and limits the surface density and at the same time also the related desorption yield to an acceptable value. A detailed discussion of ion-induced vacuum stability in a cold vacuum system can be found in Ref. [21].

2.5 ISR observations and remedies for the ion-induced pressure instability

Up to now, the ISR has been the only machine where the ion-induced pressure instability has been observed. In the ISR, the pressure rise has been observed initially at very low beam currents of only a few amperes. Following many years of intensive effort this limit could be increased to about 60A by installing additional pumps, thus reducing L and increasing S but primarily by improving systematically the surface cleanliness of all vacuum chambers. A typical example of the build-up of an unstable pressure during beam stacking is shown in Fig. 16. A consistent observation also shown in this figure is slow build-up of the pressure over many hours following the stacking of the beam which is not expected from the simple stability condition. To understand the observed slow time response of the pressure a model, which involves the interaction of the volume gas with an adsorbed surface phase, has been developed [22] which is very similar to the more recent treatment for the LHC cold bore vacuum system [23]. A further important observation has been that while a pressure instability develops, the gas composition slowly evolves from a hydrogen-dominated rest gas to a rest gas dominated by CO [24]. Since for this gas species the desorption yield is larger (larger ion mass) and the effective pumping speed smaller (smaller vacuum conductance) compared to hydrogen, the stability limit can be significantly lower.

3. CONCLUSIONS

From the ISR observations the following conclusions have been drawn [25] which may be relevant also for the design of future machines:

η(CO) for 300°C baked stainless steel chambers ranges between 2 and 4.

Vacuum chambers which have been cleaned by argon-ion glow-discharge prior to installation and which have been baked *in-situ* show η values which are reliably and permanently close to zero or even negative.

Beam pumping has been observed in many places at intermediate beam currents, particularly where the intrinsic pumping speed of the system was low and thus the relative effect of the beam larger. A safe, conservative vacuum design should, however, not be based on this transient effect.

For the LHC, it is expected that many room-temperature sections will require special measures to guarantee vacuum stability. This applies in particular to the vacuum systems for the experiments which need to be designed with adequate safety margins by making the necessary provisions for the pumping and for low desorption yields.

REFERENCES

[1] O. Gröbner et al., Vacuum 33, No.7, 397 (1983).

[2] Ch. Falland et al., VIII Int. Vacuum Congr., Cannes, September 22-26 (1980).

[3] C. Herbeaux et. al., J. Vac. Sci. Technol. A 17(2) Mar/Apr. (1999).

[4] J-P. Bojon et al., EPAC-92, Berlin, 24-28 March (1992).

[5] G.E. Fischer, R.A. Mack, J. Vac. Sci. Technol. 2 123 (1965).

[6] M. Bernardini and L. Malter, J. Vac. Sci. Technol. 2, 130 (1965).

[7] J. Gómez-Goñi, O. Gröbner and A.G. Mathewson, J. Vac. Sci. Technol. A 12 (4), Jul/Aug (1994).

[8] O. Gröbner, Vacuum 46, No 8-10, 797 (1995).

[9] P.M. Strubin and J-P. Bojon, PAC-95, Dallas (1995).

[10] M. Andritschky et al., Vacuum, 38, No 8-10, 933 (1988).

[11] F. Rieke and W. Prepejchal, PR A6, 1507 (1972).

[12] E. Fischer and K. Zankel, CERN/ISR-VA/73-52 (1973).

[13] O. Gröbner and R. Calder, PAC 73, San Francisco, 760 (1973).

[14] J.M. Laurent, private communication, 1998.

[15] A.G. Mathewson, CERN/ISR-VA/76-5, 1st March (1976).

[16] A.G. Mathewson, Vuoto, Vol. 17, No. 3, 102, July-September (1987).

[17] Original data from A.G. Mathewson compiled by I.R. Collins.

[18] R. Veness et. al., EPAC-98, Stockholm (1998).

[19] C. Benvenuti, R. Calder and N. Hilleret, IEEE Trans. on Nucl. Sci. Vol, NS-24, No. 3, June (1977).

[20] J.C. Barnard, I. Bojko and N. Hilleret, Vacuum 47, No. 4, 347, (1996).

[21] W.C. Turner, J. Vac. Sci. Technol., A 14 (4), 2026 (1996).

[22] O. Gröbner, CERN/ISR-VA/76-25, 8th June (1976).

[23] O. Gröbner, The LHC vacuum System, these proceedings.

[24] A.G. Mathewson and P. Strubin, ISR Performance Report, ISR/VA/AM/sm, 17th August (1981).

[25] E. Fischer, ISR Performance Report ISR-VA/EF/sm, 3rd October (1975).